Gaussian derivative wavelet propagation in a single scattering bubbly water beyond resonance frequency

Yves Le Gonidec

Gaussian derivative wavelet propagation in a single scattering bubbly water beyond resonance frequency

Yves Le Gonidec

1 July 2023

Univ. Rennes, CNRS, Géosciences Rennes, UMR 6118, 35000 Rennes, France
Yves.LeGonidec@univ-rennes1.fr

Abstract

Acoustic pulses transmitted across air bubbles in water are usually analyzed in the ν frequency domain to determine attenuation and phase velocity for comparison with effective models. In the present work, acoustic experiments performed beyond the bubble resonance frequency highlight an attenuation approximated to $a(\nu/\nu_{p_0})^{-y}$ with $y > 0$ and ν_{p_0} the wavelet source peak frequency, a significant shape variability of the waveform with the propagation distance x <0.74 m, and a nearly constant normalized amplitude spectrum. The amplitude spectrum can be characterized by a fractional derivative order $\gamma_x = \kappa_\gamma x$, with κ_γ a constant defined by a numerical optimization method, and a time dilation factor δ_x . The phase spectrum is shifted by $\pi\gamma_x/2$ and explains the experimental waveform changes. The phase velocity can be approximated to $\tilde{v}_0/(1 - \kappa_\gamma\tilde{v}_0/4\nu)$, where $\tilde{v}_0$ is similar to the sound speed in water. It is also shown that the waveform shape, quantified by γ_x, is correlated to the waveform amplitude. With the assumption $ayx < 0.15$, the range of applicability may be extended to the ocean water column around gas seep sites with potential interests in underwater communication.

1 Introduction

In underwater acoustics, a wave may be drastically affected by the presence of bubbles which act as strong scatterers [1]. A single bubble is characterized by a low-frequency resonance ν_r, typically 3 kHz for a 1 mm radius air bubble in water as firstly quantified in the 1930s by Minnaert and intensively considered since then [2, 7]. For a bubble cloud, the bubbly water is characterized by an effective complex wavenumber which real and imaginary parts are related to the phase velocity $v(\nu)$ and attenuation coefficient $\alpha(\nu)$, respectively. Many physical phenomena and bubble properties can be considered when modeling v and α, including multiple scattering and bubble-bubble interactions [4, 8, 15,

25, 28], encapsulating shell and bubble shape [14, 18, 23, 24] and polydispersity [11]. Because of this complexity, various experimental works have been performed since many years to measure v and α and compare the results with effective models in the frequency domain [6, 13, 17, 26, 31].

Some publications illustrate the acoustic signals in the time domain [9, 10, 22, 27]. For instance, Leroy, Strybulevych, and Page [22] show a 50 kHz acoustic pulse transmitted through a bubbly gel composed of 0.15% volume fraction of 81 μm radius bubbles: the shape of the transmitted signal is more complex than the pulse shape. A quantitative relationship between this complexity and the dispersive character of the bubbly gel is not obvious since the measurement had been performed near resonance where attenuation and phase velocity change significantly with the frequency [12]. For a weak attenuation that linearly increases with the frequency [16], waveform changes can be attributed to fractional integration effects [19]. This may be not the case in the bubbly medium at frequencies far beyond the bubble resonance frequency where the attenuation is weak but follows a decreasing trend with the frequency. In the present work, a 310 kHz acoustic pulse propagates in a bubbly water composed of roughly 0.2% volume fraction of 1.6 mm radius air bubbles ($\nu_r \simeq$2 kHz): the study focuses on analytical descriptions of phenomenological effects that affect the acoustic waveform.

The laboratory acoustic experiments are described in Section 2 to introduce qualitative changes of the acoustic waveforms associated to a propagation distance $x \leq$740 mm inside the bubbly water. In Section 3, the attenuation of the waveform amplitude as a function of x is quantified in the time domain, and α and v are measured in the frequency domain to be compared with effective models. Section 4 deals with analytical developments based on Gaussian derivative properties of a model source wavelet: fractional derivation and dilation parameters are introduced from an approximation of α at high frequencies and used to approximate v accordingly to model the acoustic waveform across the dispersive medium. The analysis is extended to the experimental waveforms where the correlation between the shape and amplitude of the waveforms is highlighted in agreement with the modeling. The range of applicability of the approach is quantified and discussed in Section 5 by considering different theoretical bubbly waters and propagation distances.

Conclusion and perspective for future studies are presented in Section 6, in particular for acoustic characterization of gas seeps in the ocean water column.

2 Description of the acoustic experiments

Two series of experiments have been performed in an acoustic tank filled with 5 m^3 of tap water: one in pure water (non-dispersive homogeneous medium) and one in bubbly water (dispersive biphasic medium).

2.1 Acoustic waveforms measured in pure water

A piezo-electric transducer, with a central frequency of 500 kHz and an active face that acts as a circular plane piston of radius R=1.5 cm, is used to emit an acoustic pulse into the so-called reference pure water. A similar transducer is placed in front of the emitter to record the transmitted acoustic signal. The waveform $W_0(t)$ recorded at the distance x_0=365 mm represents the reference signal in the following (Fig. 1a1). As a first approximation, the waveform is a Gaussian derivative wavelet (see Eq. 7) composed of 5 extrema: it is symmetric relative to the main peak which defines the center of the waveform and is arbitrary set to 1 (normalized amplitude at x_0). The signal is a superposition of plane waves with harmonic time dependence according to the Fourier transform, *i.e.*

$$\hat{W_0}(\nu) = \frac{1}{2\pi}\int_{-\infty}^{\infty} W_0(t)e^{-i2\pi\nu t}dt, \tag{1}$$

which modulus is maximum at the peak frequency ν_{p_0} $\simeq$310 kHz (Fig. 1a4). Note that the measurements are performed in the far field condition $x_0 > R^2/4\lambda$, where λ is the acoustic wavelength in water. The measurements are performed for successive positions x of the receiver (Fig. 1a2). The position is defined from the time-of-flight of the transmitted signal in water (sound speed v_0=1473 m.s^{-1}) and ranges between x_0 and x_0+840 mm. The dataset consists in 221 acoustic waveforms $W_x(t)$ acquired with a sampling rate of 10 MHz. By both correcting the waveform amplitude from the spherical divergence of the acoustic beam and time shifting the amplitude peak at t=0, the waveforms measured in pure water are all similar to $W_0(t)$ (Figs. 1a2): in particular, the symmetry of the waveform and the amplitude spectrum do not depend on the distance x as expected for a non dispersive medium (Figs. 1a3 and 1a4).

2.2 Acoustic waveforms measured in bubbly water

The dataset of the second experiment has been acquired when air bubbles are being released in the pure water to create a dispersive biphasic medium. Bubbles are released by the use of an artificial generator composed of 8 parallel identical pierced tubes, 10 cm apart, filled with air under a pressure of 1.4 bars (Fig. 2a). Each tube, 8 mm in diameter, has been pierced of 26 holes, 2 cm apart, to create a bubble cloud in the water. The distance between the acoustic emitter and the first tube is 100 mm, *i.e.* the recorded waveform at the initial position x_0 is $B_0(t) = W_0(t)$ (Fig. 1b1). The trajectory of the bubbles rising up to the surface is not straight and fluctuates in the vicinity of each tube: as a first approximation, the instantaneous bubble distribution is homogeneous. Bubbles are ellipsoidal (Fig. 2a), with half minor axes between 1 and 3 mm and an eccentricity about 1.5 (Fig. 2b). Measurements are not accurate but not critical for the present study and a bubble is approximated to a fluid sphere which radius is half the minor axis, in average normal to the acoustic beam. A log-normal distribution highlights a median value r_0=1.6 mm and a polydispersity ϵ=20% (Fig. 2c). The gas volume fraction of the biphasic medium is estimated from $\frac{4}{3}\pi r_0^3 N_b N_t/V$ where N_b $\simeq$11 is the number of bubbles in one

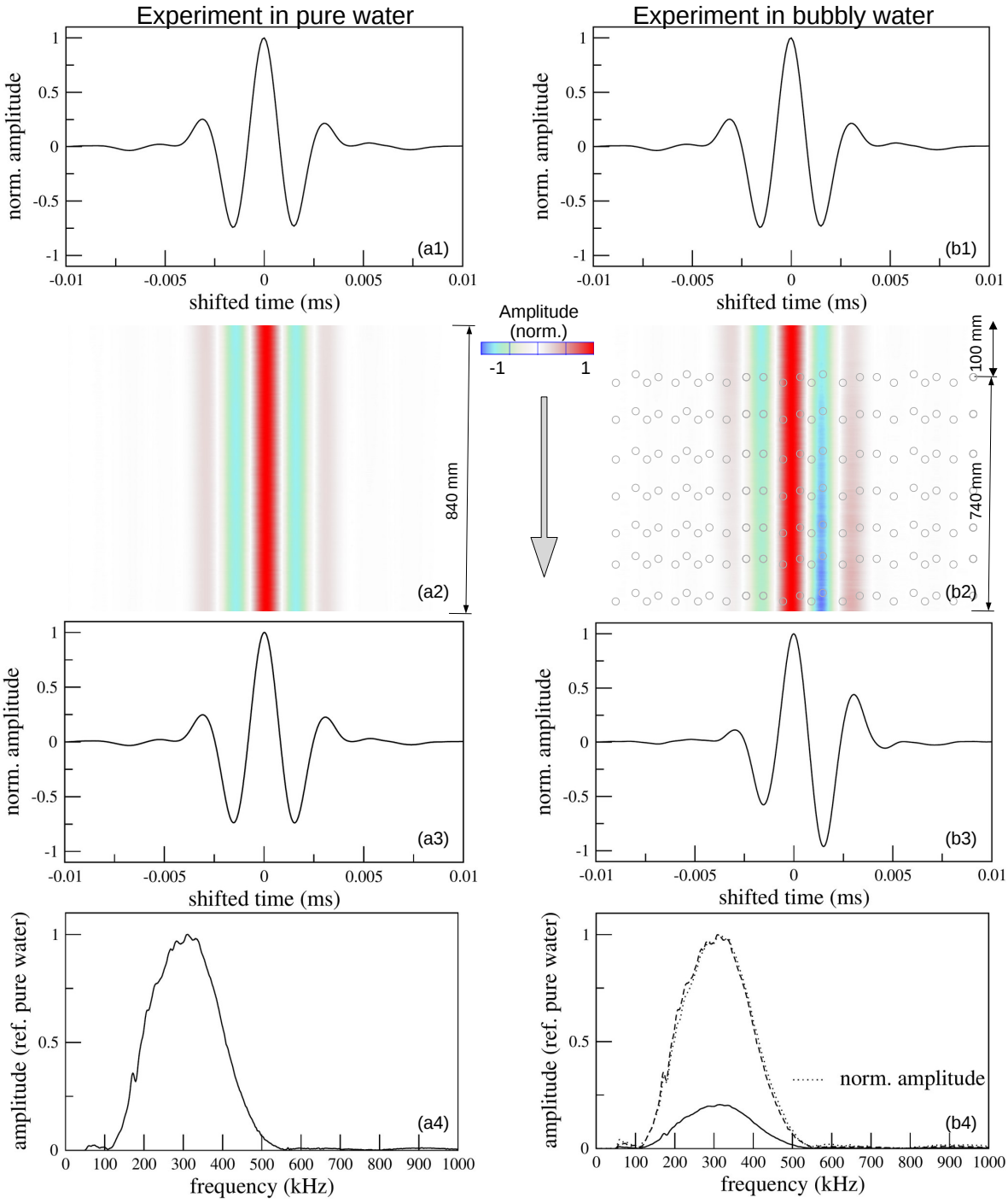

Figure 1: Experimental waveforms measured (left) in pure water and (right) in bubbly water: (a1 and b1) reference source signals and (a2 and b2) transmitted waveforms measured at 211 successive positions x. The waveforms are displayed with a normalized amplitude and an arbitrary time reference. (a3 and b3) Last transmitted waveforms and (a4 and b4) associated amplitude spectra normalized to the amplitude in pure water (solid curves). Note that the normalized amplitude spectra measured in pure and bubbly waters are similar (b4, dashed and dotted curves, respectively).

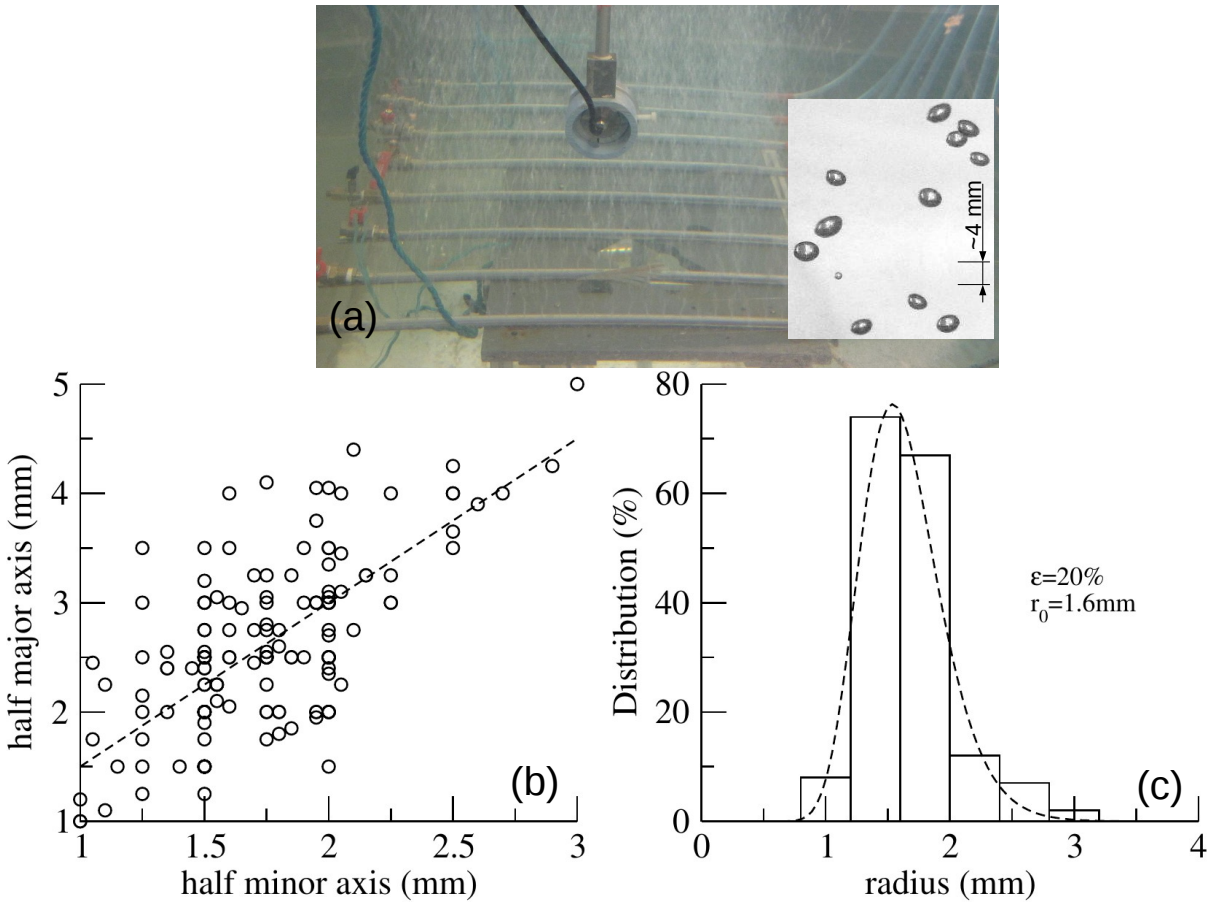

Figure 2: (a) Photographs of the 8 bubble clouds and few bubbles (inset picture). (b) Major and minor axes of elliptical bubbles (circles). (c) Experimental and log-normal (dashed curve) size distributions.

picture, N_t=8 is the number of tubes, and $V \simeq$1.5 l is the volume associated to the picture surface multiplied by the length 740 mm of bubbly water. As a rough estimate, the bubbly liquid is characterized by 0.15% volume fraction of 1.6 mm radius air bubbles with a 20% polydispersity in pure water where the sound speed is about 1473 m.s^{-1}.

The mean acoustic field is measured by averaging 200 signals that propagate through different realizations of the dynamic bubbly water. The dataset of the second experiment consists in 221 average acoustic waveforms $B_x(t)$ measured for different propagation distances x and both corrected in amplitude from the spherical spreading and time-shifted to align the amplitude peak at t=0 (Fig. 1b2). As a key observation, the waveform $B_x(t)$ is not constant with x: in particular, the symmetry is progressively lost when the propagation distance inside the bubbly water increases from 0 to 740 mm (Figs. 1b2 and 1b3) but the normalized amplitude spectrum is not modified (Fig. 1b4).

This highlights qualitative results on the continuous modification of the average acoustic waveform when the acoustic wave propagates inside the bubbly water. To better under-

stand the interaction between the acoustic wave and the bubbles, a quantitative analysis is described in the following, based on effective medium models to characterize the bubbly water in terms of attenuation and phase velocity.

3 Experimental attenuation and phase velocity

3.1 Analysis in the time domain

In pure water, the maximum amplitude $M_W(x)$ of the waveform $W_x(t)$ decreases as the spherical spreading $1/x$ (Fig. 3a, diamonds and solid curve, respectively): intrinsic attenuation of the acoustic wave propagating in the water can be neglected. In bubbly water, the decrease of the maximum amplitude $M_B(x)$ of the waveforms $B_x(t)$ (Fig. 3a, circles) is stronger than the spherical spreading when $x > 0$ which corresponds to the location of the first bubble cloud.

The attenuation of the acoustic wave can be quantified in dB according to $-20\log_{10}\left(M_B(x)/M_W(x)\right)$ (Fig. 3b, circles). Despite the average measurements performed on many realizations of bubble clouds, the results are scattered: as a first approximation, the attenuation linearly increases with x (Fig. 3b, solid line), about 5.2 dB.m^{-1} for ν_{p_0}=310 kHz. Better estimates of the bubbly water properties, *i.e.* both attenuation coefficient and phase velocity as functions of the acoustic frequency, are assessed in the frequency domain.

3.2 Analysis in the frequency domain

In pure water, an acoustic wave of angular frequency $\omega = 2\pi\nu$ propagates at a constant speed v_0 with a real wavenumber $k_0 = \omega/v_0$. In the Fourier domain, the acoustic plane-wave measured at x is given by:

$$\hat{W}_x(\nu) = \hat{W}_0(\nu)e^{i(2\pi\nu t - k_0 x)} = \hat{W}_0(\nu)e^{i2\pi\nu\left(t-\frac{x}{v_0}\right)}. \tag{2}$$

In bubbly water, the acoustic wave propagates with a frequency dependent complex wavenumber $k(\nu)$ which real and imagery parts are defined by an attenuation coefficient $\alpha(\nu)$ and a phase velocity $v(\nu)$, respectively, according to:

$$k(\nu) = \frac{2\pi\nu}{v(\nu)} - i\alpha(\nu) \tag{3}$$

and the acoustic plane-wave measured after a propagation distance x inside the bubbly water is thus given by:

$$\hat{B}_x(\nu) = \hat{B}_0(\nu)e^{i(2\pi\nu t - kx)} \tag{4a}$$

$$= \hat{B}_0(\nu)e^{-\alpha x}e^{i2\pi\nu\left(t-\frac{x}{v}\right)} \tag{4b}$$

$$= \hat{W}_x(\nu)e^{-\alpha x}e^{i2\pi\nu\left(\frac{x}{v_0}-\frac{x}{v}\right)}. \tag{4c}$$

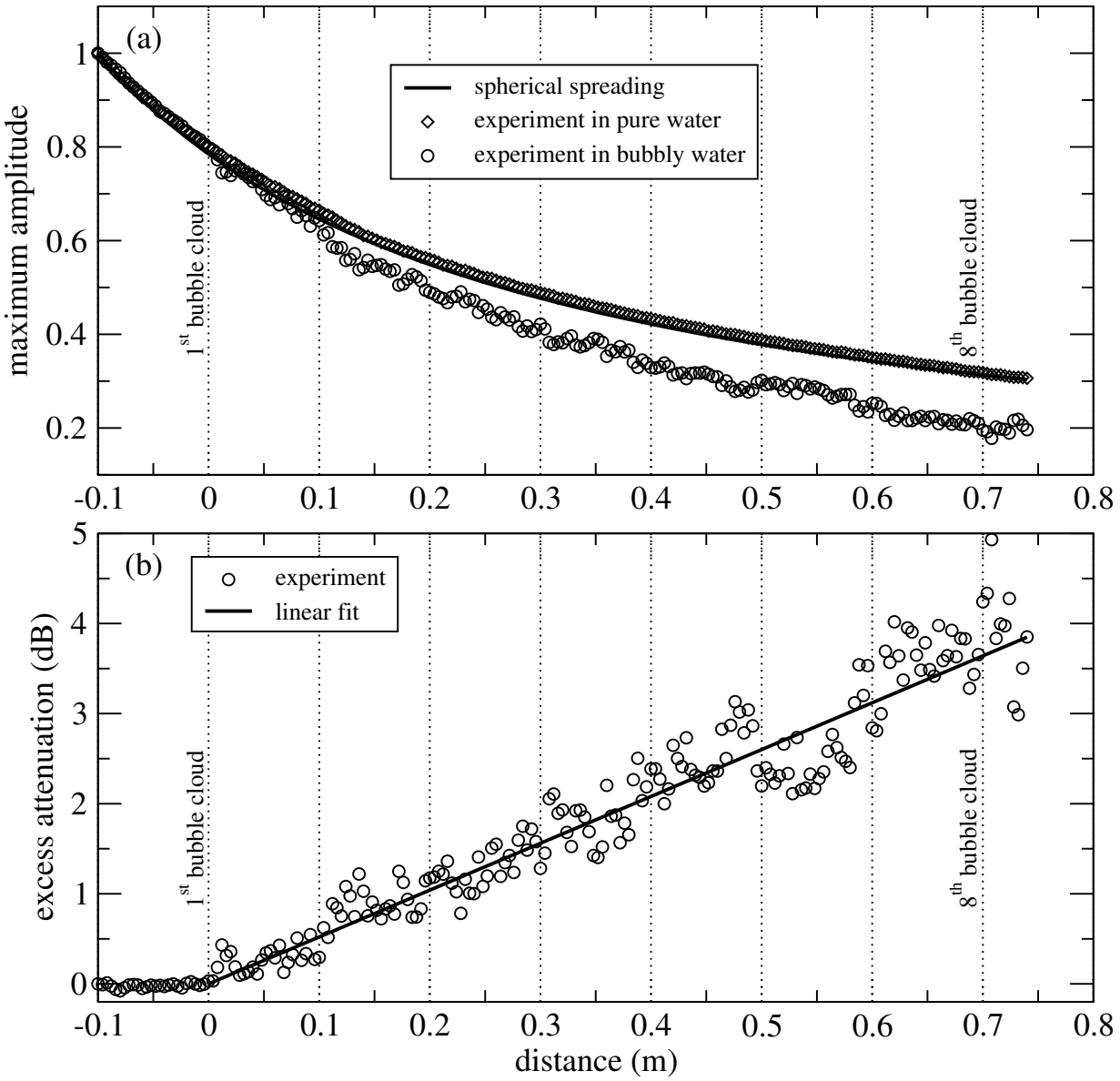

Figure 3: (a) Decreasing trend of the waveform amplitude in pure water (diamonds), in accordance with the spherical spreading of the acoustic wave (solid curve), and in bubbly water (circles) as a function of the distance x. (b) Difference in attenuation between the bubbly and pure waters, *i.e.* excess attenuation in dB induced by the bubbles as a function of x (circles), and linear fit (solid line).

The attenuation coefficient is related to the ratio of the moduli $|\hat{B}_x(\nu)|$ and $|\hat{W}_x(\nu)|$ and the phase velocity to the phase shift $\Delta\Phi = arg(\hat{B}_x(\nu)) - arg(\hat{W}_x(\nu))$ which gives:

$$\alpha(\nu) = -\frac{1}{x}\ln\frac{|\hat{B}_x(\nu)|}{|\hat{W}_x(\nu)|} \tag{5a}$$

$$v(\nu) = \frac{xv_0 2\pi\nu}{x2\pi\nu - v_0\Delta\Phi}. \tag{5b}$$

For frequencies close to $\nu_{p_0} \gg \nu_r$, the experiments highlight very weak dependencies of both α and v with ν (Fig. 4, circles).

3.3 Effective medium modeling of the bubbly water

The bubbly water is a biphasic system composed of air bubbles in a fluid matrix and is characterized by a theoretical effective complex wavenumber $k(\nu)$ related to the physical properties of the medium by the use of an effective medium modeling.

The model developed by Foldy [12] is widely used in the 'Independent Scattering Approximation' for dilute systems characterized by both a mean distance d between the bubbles much larger than the acoustic wavelength λ and isotropic scatterers with a radius $r < \lambda$. In this case, the polydisperse bubbly water is modeled by the effective complex wavenumber $k_F^2 = k_0^2 + 4\pi\int N(r)H(r)dr$. The term $N(r)$ is the log-normal distribution of the bubble size and $H(r)$ the far-field isotropic scattering amplitude of a single bubble [5, 32] characterized by the so-called Minnaert frequency ν_r. Note that for the radius r_0=1.6 mm, a single bubble resonates at $\nu_r \simeq$2 kHz, which is much lower than the peak frequency ν_{p_0}=310 kHz of the reference source signal $B_0(t)$.

In the model developed by Lax [20], the isotropic scattering amplitude H is replaced by the forward scattering amplitude H_0 of a fluid sphere in order to take anisotropic scatterers into account when $\lambda < r$. The wavenumber is given by

$$k_L^2 = k_0^2 + 4\pi\int N(r)H_0(r)dr \tag{6}$$

where $H_0(r)$ is a complex function that depends on the Legendre polynomials and the Neumann and Bessel functions [3].

The complex wavenumbers are computed by considering the physical parameters of the experiment, including the median bubble radius r_0=1.6 mm and the polydispersity ϵ=20%: only the volume fraction initially estimated about 0.15% has been increased to ϕ=0.2% to better fit the model and experimental results. The modeled wavenumber based on k_F predicts an attenuation that strongly depends on the frequency and underestimates the measurements (Fig. 4a, dashed curve): for frequencies as high as ν_{p_0}=310 kHz, air bubbles with r_0=1.6 mm can not be approximated to isotropic scatterers and the Foldy's model is not adapted for the present case study. The modeled attenuation α and phase velocity v based on k_L are both in good agreement with the data (Figs. 4a and b, solid curves). In particular, the model correctly predicts the weak decrease of the attenuation coefficient

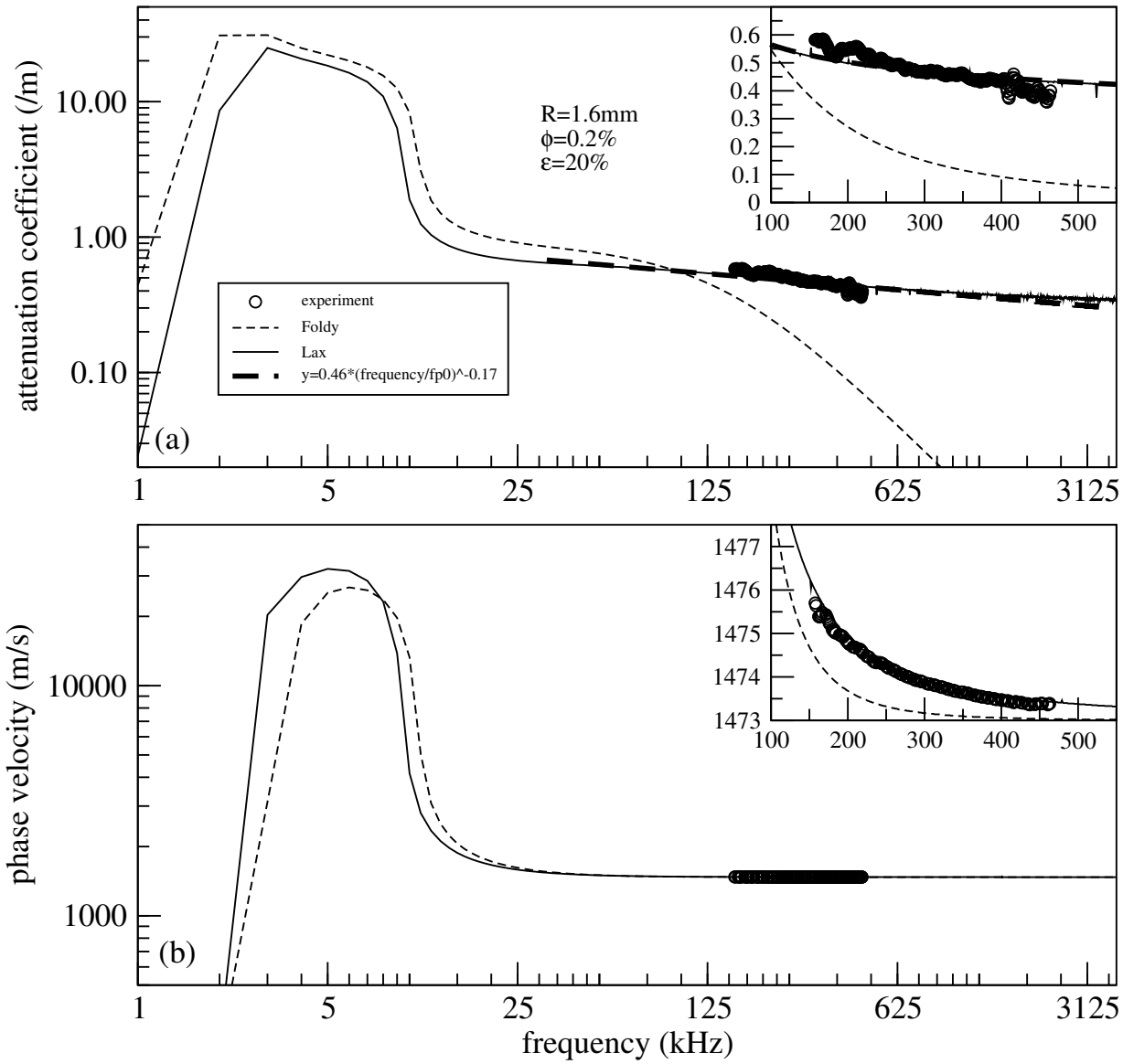

Figure 4: (a) Experimental attenuation coefficient and (b) phase velocity measured with a high frequency (peak frequency ν_0=310 kHz) acoustic pulse propagation across 740 mm of bubbly water (circles), and predicted by effective models by Foldy (dashed curve) and Lax (thin curve). The attenuation follows a power law of frequency well above resonance with an approximation determined in the dominant frequency range of the Gaussian derivative source wavelet (dashed line).

with the frequency. This means that bubbles act as anisotropic scatterers in the biphasic medium where multiple scattering can be neglected.

4 Modeling based on a Gaussian derivative source wavelet

4.1 Fractional derivation and dilation factors based on $\alpha(\nu)$

The reference source signal $B_0(t)$ is similar to a Gaussian derivative wavelet with a derivative order β_0=4 [21]:

$$B_0(t) \sim S_0(t) \equiv \frac{d^{\beta_0}}{dt^{\beta_0}} e^{-\pi^2 \nu_0^2 (t-\tau_0)^2} \tag{7}$$

characterized by 5 extrema and symmetric relative to the maximum peak located at time τ_0, and a natural frequency

$$\nu_0 = \nu_{p_0} \sqrt{2/\beta_0} \tag{8}$$

where ν_{p_0}=310 kHz is the peak frequency. In the frequency domain, the wavelet can be expressed by

$$\hat{S}_0(\nu) = \left(\frac{\nu^2}{\nu_{p_0}^2} e^{1-\frac{\nu^2}{\nu_{p_0}^2}} \right)^{\frac{\beta_0}{2}} e^{i\left(-2\pi\nu\tau_0 + \pi\frac{\beta_0}{2}\right)} \tag{9}$$

and includes the normalization factor of the Gaussian derivative function [30], *i.e.* $|\hat{S}_0(\nu_{p_0})|$=1. Inside the bubbly water, the amplitude spectrum of the Fourier transform of the waveform $B_x(t)$

$$|\hat{B}_x(\nu)| = e^{-\alpha(\nu)x} \left(\frac{\nu^2}{\nu_{p_0}^2} e^{1-\frac{\nu^2}{\nu_{p_0}^2}} \right)^{\frac{\beta_0}{2}} \tag{10}$$

directly leads to $\alpha(\nu_{p_0}) = -\ln|\hat{B}_x(\nu_{p_0})|/x$, and the phase spectrum

$$\arg\left(\hat{B}_x(\nu)\right) = -2\pi\nu \left(\tau_0 + \frac{x}{v(\nu)} \right) + \frac{\pi}{2}\beta_0 \tag{11}$$

is characterized by a constant phase shift $\frac{\pi}{2}\beta_0$.

A common assumption for dispersive media is an attenuation that depends on the power of frequency, where the power value is not necessarily an integer [16]. For the bubbly water, the attenuation decreases with the frequency well above resonance (Fig. 4a, dashed bold curve) and can be approximated by a power law

$$\alpha(\nu) \sim \tilde{\alpha}(\nu) = a \left(\frac{\nu}{\nu_{p_0}} \right)^{-y} \tag{12}$$

with a=0.46 m^{-1} and y=0.17 based on the modeling result in the dominant frequency range of the Gaussian derivative source wavelet. This quantifies a weak decreasing trend

of the attenuation with the frequency. But considering a power law for α in the amplitude spectrum (eq. 10) is not an easy task to go further into the analytical developments and an approximation of the form $\alpha(\nu) \sim \tilde{\alpha}(\nu) = a - b \ln \frac{\nu}{\nu_{p_0}}$ would be better suited to that aim. The equivalence between the frequency decreasing trends of the two approximations leads to

$$b \simeq ay \tag{13}$$

in the close vicinity of ν_{p_0}, which gives $b \simeq$0.077 m^{-1}. In this case, the amplitude spectrum can be approximated to

$$|\hat{B}_x(\nu)| \sim |\hat{\tilde{B}}_x(\nu)| = e^{-ax}\nu^{bx}\left(\frac{\nu^2}{\nu_{p_0}^2}e^{1-\frac{\nu^2}{\nu_{p_0}^2}}\right)^{\frac{\beta_0}{2}} \tag{14}$$

suggesting that the dispersive medium may act as a derivative filter which should also impact the phase velocity, as discussed in the next section. In the close vicinity of ν_{p_0}, it can be shown analytically that

$$|\hat{\tilde{B}}_x(\nu)| = A_x\left(\frac{\nu^2}{\nu_{p_x}^2}e^{1-\frac{\nu^2}{\nu_{p_x}^2}}\right)^{\frac{\beta_0+bx}{2}} \tag{15}$$

with

$$A_x = e^{-x(a+\frac{b}{2})}\nu_{p_0}^{bx}\left(\frac{\beta_0+bx}{\beta_0}\right)^{\frac{\beta_0+bx}{2}}. \tag{16}$$

The amplitude spectrum of $B_x(t)$ is thus similar to the amplitude spectrum of a new Gaussian derivative function characterized by a derivative order $\beta_0 + bx$ and a peak frequency

$$\nu_{p_x} = \nu_{p_0}\sqrt{\frac{\beta_0+bx}{\beta_0}} = \nu_0\sqrt{\frac{\beta_0+bx}{2}}. \tag{17}$$

In one hand, the dispersion of the acoustic wave linearly increases the peak frequency from ν_{p_0}=310 kHz when x=0 to 312.5 kHz when x=740 mm, a very weak frequency shift (lower than 0.1 %) in agreement with the experimental observations. In the other hand, the derivative order increases from β_0=4 when x=0 to 4.07 when x=740 mm, not in agreement with the lost of symmetry of the reference signal observed in the experiments (see Fig. 1). This means that the bubbly water can not be approximated to a simple derivative filter.

Actually, the natural frequency of the new Gaussian derivative wavelet appears to depend on x *via*

$$\nu_{p_x} = \nu_{0_x}\sqrt{\frac{\beta_x}{2}} \tag{18}$$

associated to the derivative order

$$\beta_x = \frac{\nu_0^2}{\nu_{0_x}^2}(\beta_0+bx) = \frac{\beta_0+bx}{\delta_x^2} \tag{19}$$

where δ_x is a time-dilation factor. As a result, the peak frequency

$$\nu_{p_x} = \nu_{p_0}\delta_x\sqrt{\frac{\beta_x}{\beta_0}} \tag{20}$$

and the amplitude spectrum

$$|\hat{\tilde{B}}_x(\nu)| = A_x\left[\left(\frac{\nu^2}{\nu_{p_x}^2}e^{1-\frac{\nu^2}{\nu_{p_x}^2}}\right)^{\frac{\beta_x}{2}}\right]^{\delta_x^2} \tag{21}$$

depend on δ_x and β_x instead of the parameter b (eq. 19). Interestingly, by introducing here the derivative order

$$\gamma_x = \beta_x - \beta_0, \tag{22}$$

this can be generalized to

$$|\hat{\tilde{B}}_x(\nu)| = A'_x\left[\left|\hat{S}_0\left(\frac{\nu}{\delta_x}\right)\right|\left(\frac{\nu}{\delta_x}\right)^{\gamma_x}\right]^{\delta_x^2} \tag{23}$$

with

$$A'_x = e^{-ax-\frac{\beta_0}{2}\left(\delta_x^2-1\right)}\nu_{p_0}^{\beta_0\left(\delta_x^2-1\right)}\delta_x^{(\beta_0+\gamma_x)\delta_x^2}. \tag{24}$$

This puts in evidence that the dispersive medium induces both time derivation and dilation effects which compensate in the amplitude spectrum of the transmitted signal $B_x(t)$.

If $bx \ll \beta_0$, a condition satisfied in the present case study where $\tilde{\alpha}(\nu)$ is nearly a constant in the dominant frequency range of the source wavelet, the analytical approach gives

$$\delta_x^2\left(\beta_0+\gamma_x\right) \simeq \beta_0 \tag{25}$$

and $\nu_{p_x} \simeq \nu_{p_0}$ in agreement with the experiments. The trivial solution $\gamma_x = 0$ and $\delta_x = 1$ is observed in the experiments only at x=0: to quantify δ_x and γ_x associated to waveform changes inside the dispersive medium, an analytical approximation of the phase velocity is required.

4.2 Corresponding analytical approximation of $v(\nu)$

The amplitude spectrum of the signal $B_x(t)$ measured inside the bubbly water is similar to $|\hat{\tilde{B}}_x(\nu)|$ characterized by both the fractional derivative order γ_x and the dilation factor δ_x applied to the Gaussian derivative source wavelet $S_0(t)$. As a first approach, the associated phase spectrum is written as

$$\arg\left(\hat{\tilde{B}}_x(\nu)\right) = \arg\left(\hat{S}_0\left(\frac{\nu}{\delta_x}\right)\right) + \frac{\pi}{2}\gamma_x - 2\pi\nu T'_x \tag{26}$$

where the travel time $T'_x = \frac{x}{v_0} + \tau'_x$ corresponds to the sum of the travel time in pure water and a supplementary time shift τ'_x to align the maximum amplitudes of $\tilde{B}_x(t)$ and $B_x(t)$. The approximation $\arg\left(\hat{B}_x(\nu)\right) \sim \arg\left(\hat{\tilde{B}}_x(\nu)\right)$ leads to the phase velocity approximation

$$v(\nu) \sim \tilde{v}(\nu) = v_0\left[1 + \frac{v_0}{x}\left(\tau_0\frac{1-\delta_x}{\delta_x} + \tau'_x - \frac{\gamma_x}{4\nu}\right)\right]^{-1}. \tag{27}$$

Actually, τ'_x depends on δ_x and γ_x and can be replaced by an equivalent time shift τ_x to write the phase spectrum as

$$\arg\left(\hat{\tilde{B}}_x(\nu)\right) = \arg\left(\hat{S}_0\left(\nu\right)\right) + \frac{\pi}{2}\gamma_x - 2\pi\nu\left(\frac{x}{v_0} + \tau_x\right) \tag{28}$$

and the phase velocity becomes

$$\tilde{v}(\nu) = v_0\left[1 + \frac{v_0}{x}\left(\tau_x - \frac{\gamma_x}{4\nu}\right)\right]^{-1}. \tag{29}$$

It is of first importance to highlight here that waveform changes measured inside the dispersive medium are related to the derivative order γ_x applied to the phase spectrum of the source signal. In these analytical approximations, the equivalent medium is characterized by an effective velocity defined by

$$\tilde{v}_0 = \lim_{\nu\to+\infty}\tilde{v}(\nu) \tag{30}$$

and a phase velocity $\tilde{v}(\nu)$ that should not depend on the propagation distance x, *i.e.* it is expected that $\gamma_x = \kappa_\gamma x$ and $\tau_x = \kappa_\tau x$ where the coefficients κ_γ and κ_τ are unknown.

Analytical developments to express γ_x and τ_x with respect to x are not straightforward. Instead, an optimization approach has been developed, based on a simulated annealing method to optimize the normalized correlation coefficient between $B_x(t)$ and $\tilde{B}_x(t)$ when the source signal is the theoretical wavelet $S_0(t)$ (peak frequency ν_{p_0}=310 kHz and derivative order β_0=4). The attenuation coefficient is approximated to $\tilde{\alpha}(\nu)$ and the phase velocity $v(\nu)$ is defined by the complex effective wavenumber $k_L(\nu)$. The numerical optimization, performed for propagation distances between 0 and 740 mm ($x \leq$0 stands for propagation in water) highlights that κ_γ=0.94 m^{-1} and κ_τ=0.33 μs.m^{-1} (Figs.5a and b, respectively).

As a result, the effective and phase velocities actually do not depend on x and can be expressed as

$$\tilde{v}_0 = \frac{v_0}{1 + v_0\kappa_\tau} \tag{31}$$

which is about $\tilde{v}_0 \simeq$1472.3 m.s^{-1} close to the sound speed in water, and

$$\tilde{v}(\nu) = \tilde{v}_0\left[1 - \frac{\tilde{v}_0\kappa_\gamma}{4\nu}\right]^{-1} \tag{32}$$

which is the analytical approximation of the phase velocity when the attenuation coefficient depends on ν^{-y} with $1 > y > 0$.

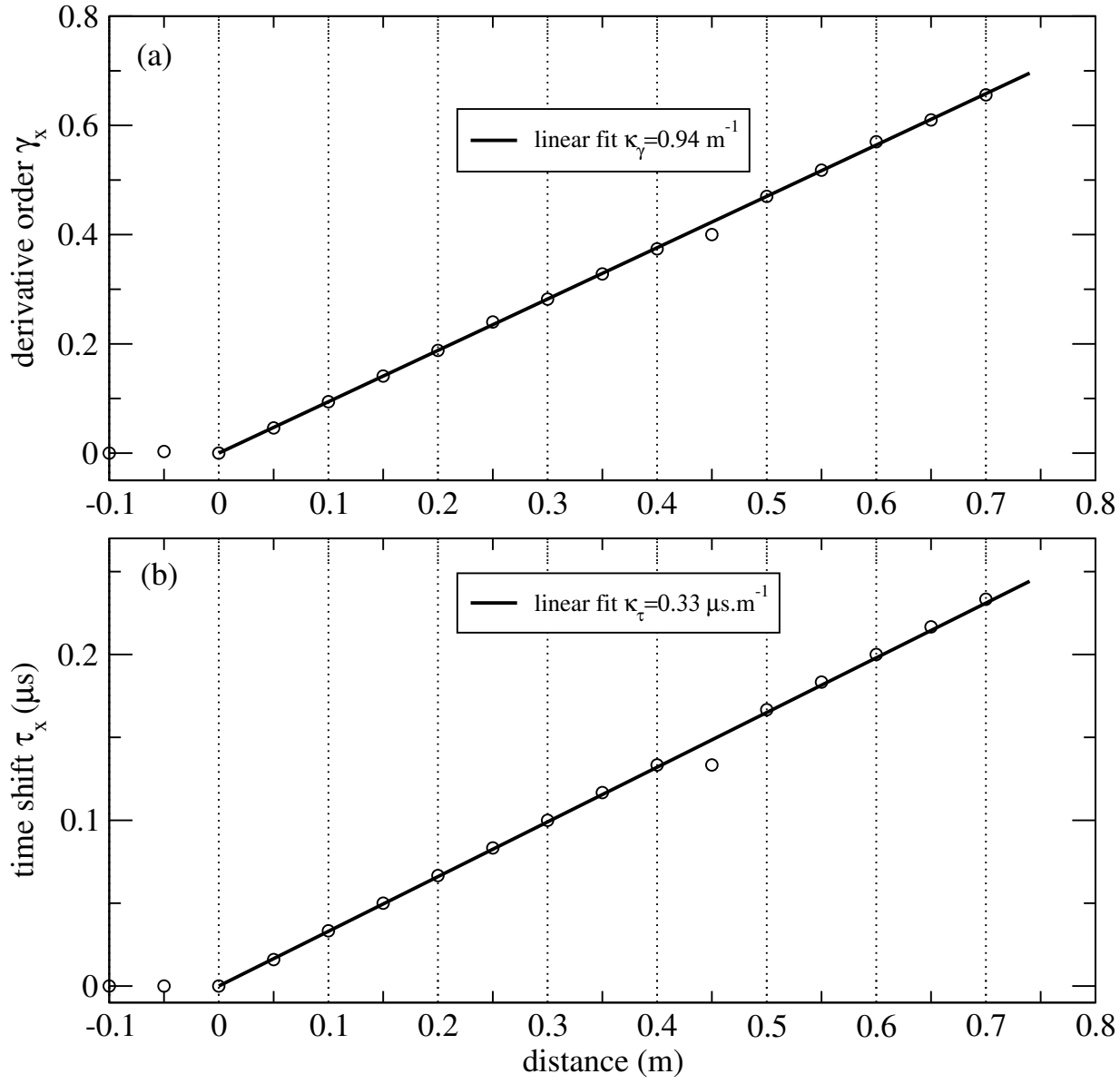

Figure 5: (a) Derivative order and (b) time shift of the optimized waveform $\tilde{B}_x(t)$ that best fits the acoustic waveform $B_x(t)$ measured at different distances inside the bubbly water (circles), and linear fits (solid lines).

4.3 Acoustic waveform modeling

The attenuation coefficient $\bar{\alpha}(\nu)$ (Fig. 6a1) and phase velocity $\bar{v}(\nu)$ (Fig. 6a2) that characterize the bubbly water effective properties are used to model the propagation of an acoustic source signal. The source signal is the theoretical wavelet $S_0(t)$ (Fig. 6b1). Changes of the waveforms with the propagation distance x (Fig. 6b2) are modeled by a simple phase shift $\pi\gamma_x/2$ that linearly increases with x with the factor κ_γ.

The waveform at x=740 mm illustrates the very good agreement with the waveform based on the complex wavenumber of the Lax's effective model (Fig. 6b3). Note that in this theoretical approach, the attenuation coefficient can be assessed by performing series of optimization procedures at x=740 mm (large distance to improve the result accuracy) without the limitation $bx \ll \beta_0$ and averaging the results based on eq. 19 to determine b: the parameter a can be assessed from the amplitude spectrum at the peak frequency.

4.4 Application to experimental signals measured across a bubbly water

The source signal is the experimental signal $B_0(t)$ (see Figs. 1b1 and 1b4). According to the previous theoretical developments, the amplitude spectrum of the transmitted signal $B_x(t)$ is similar to the one of the source signal as observed from the experimental measurements, and the phase spectrum is the one of the source signal plus a phase shift $\pi\gamma_x/2$. The aim is characterizing the experimental waveform changes across the bubbly water by the use of γ_x defined from an optimization procedure.

As a first approximation, the result of the optimization is a linear increasing trend of the derivative order with x (Fig. 7a, circles): γ_x=1.1x in agreement with the theoretical developments based on a Gaussian derivative source wavelet (Fig. 7a, solid and dashed lines, respectively). This derivative order is applied to the signal $B_0(t)$ as a phase shift $\frac{\pi}{2}\gamma_x$ to model the waveforms across the bubbly water (Figs. 7b2), with a very good agreement with the measurements (see Fig. 1b2 and the particular case at x=740 mm displayed in Fig. 7b3).

Fluctuations of the experimental γ_x are related to the dynamic of the bubbly water that can also be observed from the waveform amplitude analyzed in the time domain (Section III.A, Fig. 3b, circles). Interestingly, both this attenuation and γ_x highlight a peak and a drop located at about x=10 mm and 550 mm, respectively: this suggests a correlation between these two attributes, with a nearly constant ratio about 0.2 (Fig. 8, circles). From the theoretical developments, the amplitude is quantified by the factor A_x and gives the linear fitted attenuation $-20\log_{10} A_x$=4x: the ratio between the derivative order γ_x and this attenuation is a constant about 0.23, in agreement with the experimental results (Fig. 8, dashed line).

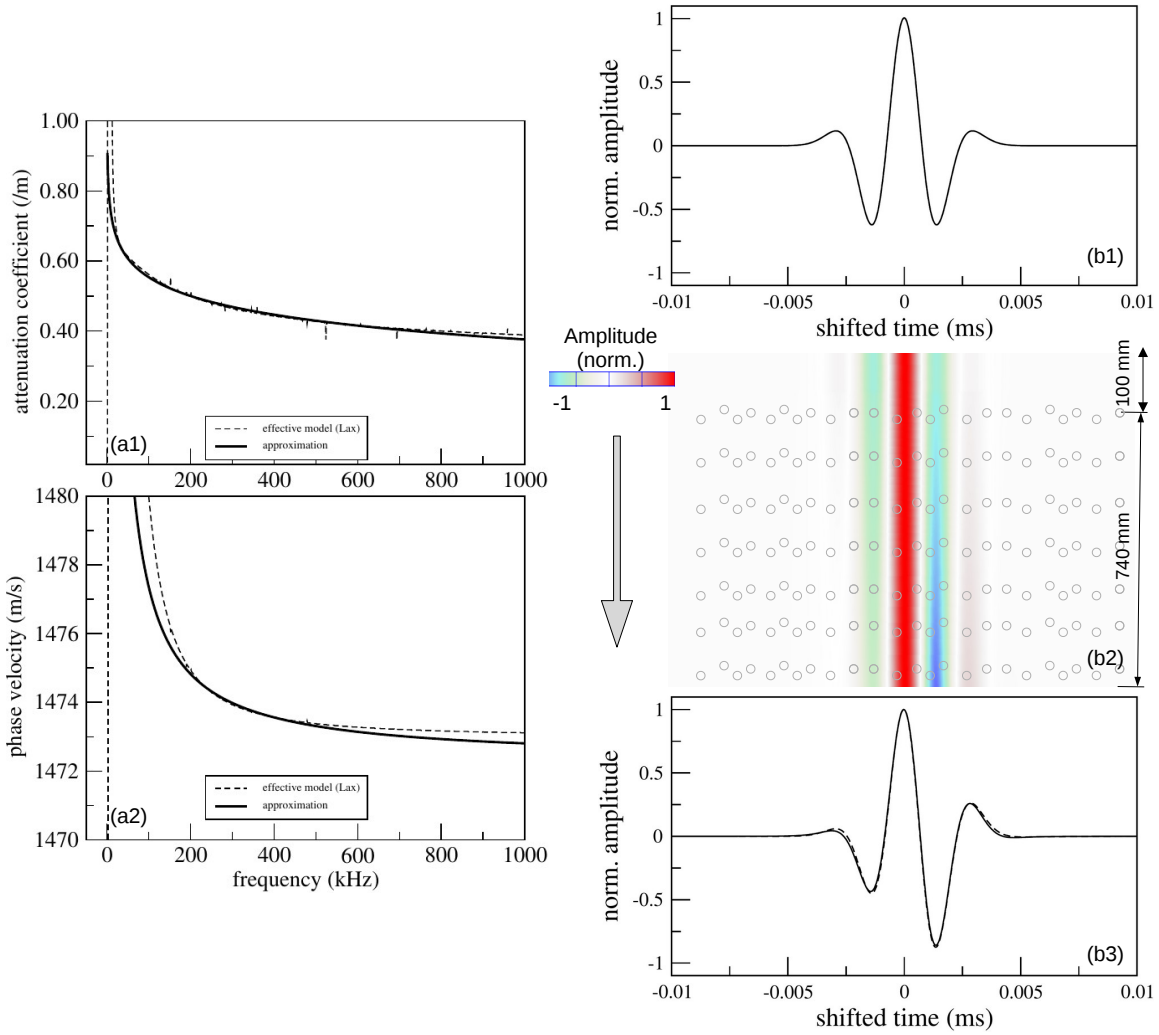

Figure 6: (a1-a2) Attenuation coefficient $\tilde{\alpha}(\nu)$ and phase velocity $\tilde{v}(\nu)$ (solid curves) used to approximate the effective model (dashed curves) based on Gaussian derivative function properties. (b1) Theoretical source wavelet $S_0(t)$ defined as a Gaussian derivative function with β_0=4. (b2) Modeling of the waveforms across the dispersive medium based on the derivative order γ_x (see Fig. 5a) applied to the phase of $S_0(t)$. (b3) Last waveform associated to $\gamma_x \simeq 0.7$ (solid curve) and waveform associated to the effective wavenumber (dashed curve).

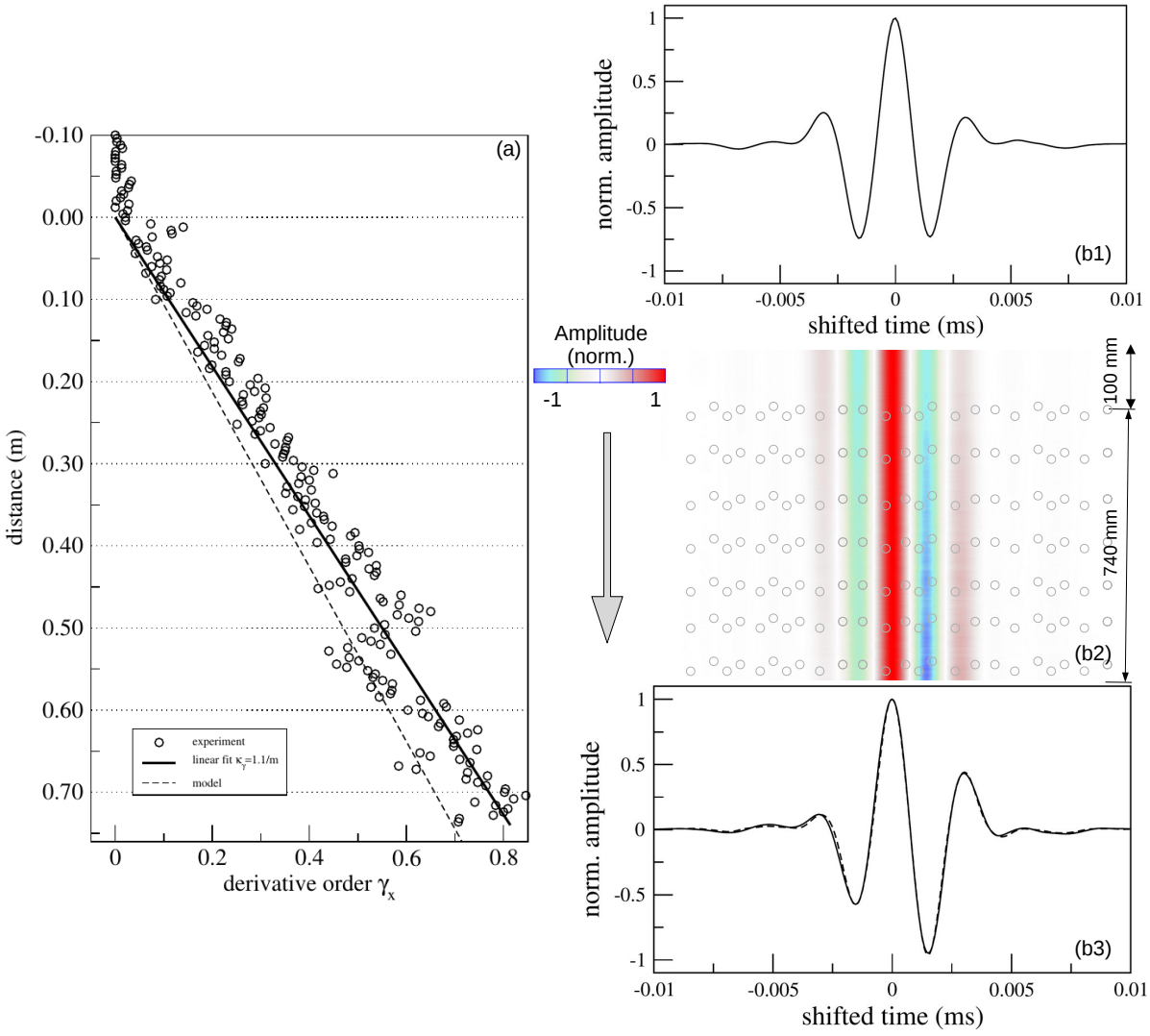

Figure 7: (a) Experimental derivative order γ_x across the bubbly water (circles): linear fits for the dynamic and theoretical static dispersive media (solid and dashed lines, respectively). (b1) Experimental source signal $B_0(t)$. (b2) Modeling of the waveforms across the dispersive medium based on the derivative order γ_x (a) applied to the phase of $B_0(t)$. (b3) Last waveform associated to $\gamma_x \simeq 0.7$ (solid curve) and waveform associated to the effective wavenumber (dashed curve).

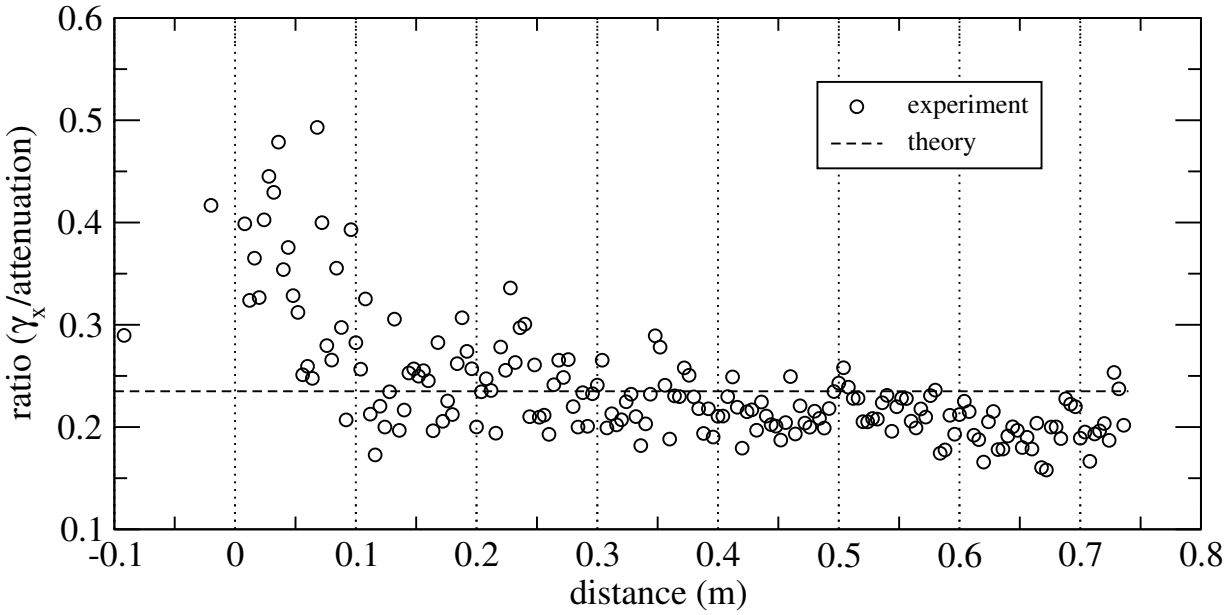

Figure 8: Experimental ratio (circles) between the derivative order γ_x and the attenuation of the waveform amplitude (Fig. 3b) as a function of the propagation distance inside the bubbly water, and theoretical ratio (dashed line) based on a Gaussian derivative source wavelet.

5 Insights into the range of applicability of the fractional derivative approximation

According to the analytical developments presented in the previous section, the effect of the attenuation coefficient on the normalized amplitude spectrum can be neglected if $bx << 1$ and the phase spectrum simply shifted by $\pi\gamma_x/2$. The approximation is in agreement with the experimental results for distances x in the range 0-0.74 m and for a volume fraction ϕ=0.2 % of r_0=1.6 mm radius bubbles. In order to discuss the range of applicability of the approach, some insights can be provided based on a theoretical extension of these experimental parameters.

The first consideration deals with the attenuation parameter b that depends on r_0 and ϕ. The range of applicability of the approximation can be estimated for a large range of bubbly waters from the normalized correlation coefficient between the theoretical acoustic waveform (signal $\mathcal{B}_x$) based on the complex effective wavenumber and the optimized derivative wavelet (signal $\tilde{\mathcal{B}}_x$). Note that increasing the bubble radius is similar, as a first approximation, to a relative decrease of the acoustic frequency band. A numerical analysis has been performed for x=1 m on 100 different bubbly waters with r_0 in the range 0.4-4 mm and ϕ in the range 0.05-0.5 % (Fig. 9a1). As a first approach, correlation coefficients better than 0.99 are considered as good derivative wavelet approximations. This is illustrated by the theoretical and approximated waveforms (Fig. 9a2, solid and dashed curves,

respectively) associated to r_0=1.2 mm and ϕ=0.25 % (Fig. 9a1, star): the correlation is 0.992 for an attenuation coefficient approximated by a frequency power law with y=0.17 and a=0.81 m^{-1}, which corresponds to $b \simeq ay$=0.14 m^{-1} (Fig. 9a3), and a phase velocity (Fig. 9a4) approximated by eq. 29 with the derivative parameter $\kappa_\gamma = 1.97$ and effective velocity $\tilde{v_0}$ =1472.61 m.s^{-1}. As a result, the range of applicability of the approximation corresponds to $0.25r_0 - 0.1 > \phi$ where the condition on the attenuation is quantified by b <0.15 m^{-1}.

The second consideration deals with the effect of the propagation distance x. For x=10 m, the map of correlation coefficients better than 0.99 is limited to low volume fractions of large bubbles (Fig. 9b1). In this case, the theoretical and approximated waveforms (Fig. 9b2, solid and dashed curves, respectively) for r_0=3.6 mm and ϕ=0.10 % (Fig. 9b1, star) are associated to a correlation of 0.998, y=0.11 and a=0.09 m^{-1}, which corresponds to b=0.01 m^{-1} (Fig. 9b3), and a phase velocity (Fig. 9b4) with $\kappa_\gamma = 0.1$ and $\tilde{v_0}$ =1471.46 m.s^{-1}. The condition of applicability of the results at large distances is in agreement with the previous consideration and it is important to note the dependency of the pulse shape with bx (Figs. 9a2 and b2 for bx=0.15 and 0.1, respectively).
As described above, the waveform of the signal changes from a symmetrical (source wavelet with β_0=4) to an asymmetrical shape when x increases. Interestingly, distances defined by $\pi\gamma_x = \pi\kappa_g x = 4\pi n$, where n is an integer, may correspond to symmetrical waveforms similar to the source wavelet shape, every 40 meters for r_0=3.6 mm and ϕ=0.10 %. But this case corresponds to bx >0.4 and is out of the applicability range of the approximation: in particular, the best fit between the waveforms would give δ_x=0 in disagreement with $\kappa_\gamma x$=4. Instead, the theoretical shape of the signal can be modeled at the particular position x=40 m: its frequency content has changed across the bubbly water and its shape is characterized by an additional negative peak of weak amplitude but even so, it is similar, as a first approximation, to the shape of the source wavelet (inset of Fig. 9b2, solid and dotted curves, respectively), in agreement with the prediction based on the analytical developments.

6 Conclusion

The present work describes both acoustic experiments and analytical developments to quantify waveform changes of a pulse (peak frequency ν_{p_0}=310 kHz) that propagates (distance $x \leq$740 mm) inside a bubbly water composed of air bubbles (radius 1.6 mm, gas volume fraction 20%). This corresponds to high frequency acoustic experiments in a single scattering dispersive medium. In the time domain, the decrease of the waveform amplitude with x is quantified by attenuation properties and qualitatively associated to changes of the waveform shape. In the frequency domain, the amplitude spectrum is nearly constant and does not depend on x. Effective medium theories are used to define the attenuation coefficient $\alpha(\nu)$ and phase velocity $\alpha(\nu)$ in agreement with the experimental results. In the high frequency range defined by the acoustic pulse, $\alpha(\nu)$ is nearly constant. In the framework of Gaussian derivative functions with a source wavelet characterized by a derivative

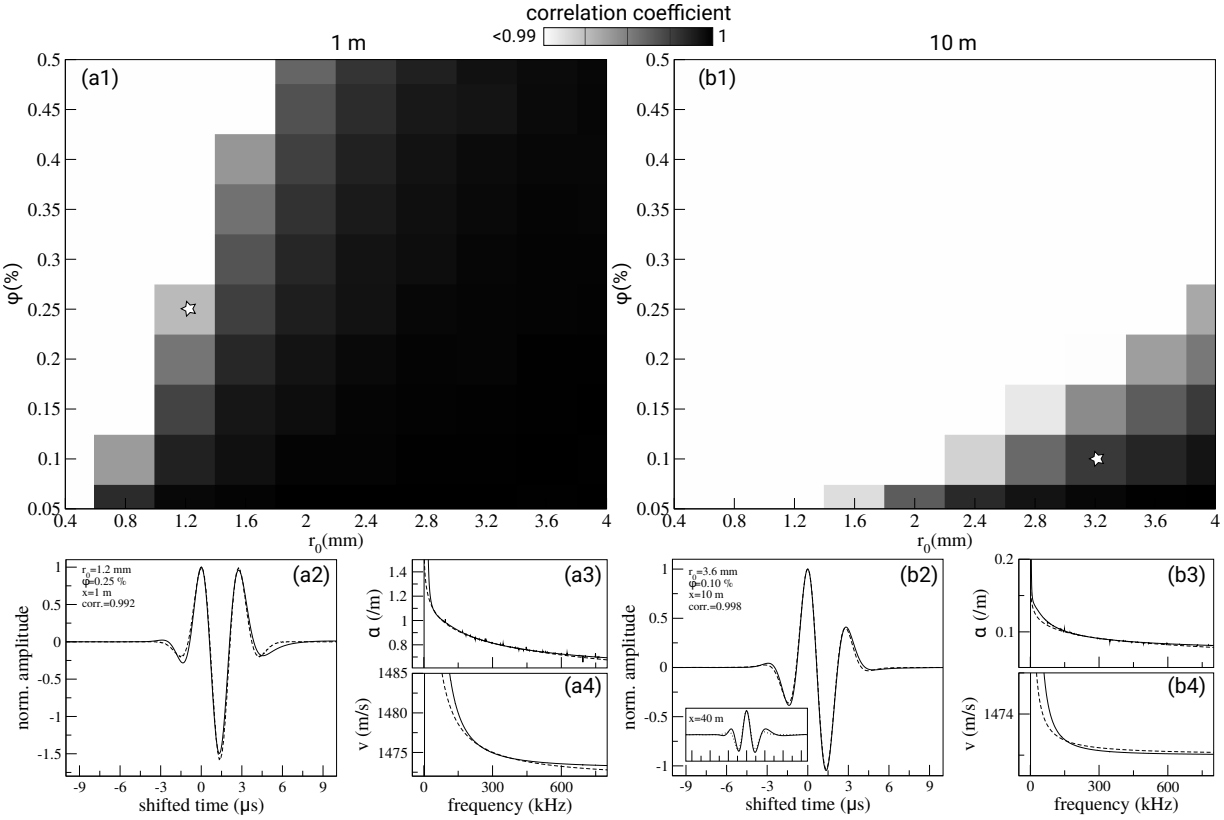

Figure 9: (a1 and a2) Maps of normalized correlation coefficients for x=1 and 10 m, respectively (best correlation in black). (a2 and b2) Waveforms of the acoustic signals modeled with the Lax's model (solid curves) for a volume fraction ϕ of r_0 radius bubbles, identified on the maps by the stars, and approximations (dashed curves). Attenuation (a3 and b3) and phase velocity (a4 and b4) associated to the Lax's model (solid line) and approximations (dashed curves). The approximations are defined in the limited frequency range of the Gaussian derivative source wavelet. (b2, inset) Shape similarity between the source wavelet (dotted curve) and modeling at x=40 m (solid curve).

order β_0=4, it is demonstrated that $\tilde{\alpha}(\nu)$ acts as a fractional derivative order $0 \leq \gamma_x \leq 0.8$ and a dilation factor $\delta_x \simeq \sqrt{\beta_0/(\beta_0+\gamma_x)}$. A numerical optimization method highlights that $\gamma_x = \kappa_\gamma x$, with κ_γ=0.94 m^{-1}. The approximation of the associated phase velocity can be written as $\tilde{v}(\nu) = \tilde{v}_0/(1-\tilde{v}_0\kappa_\gamma/4\nu)$ where $\tilde{v}_0$ is close to the sound speed in water. Based on the experimental measurements, it is also shown that the waveform shape quantified by the derivative order γ_x is proportional to the waveform amplitude which decreases with the propagation distance x across the dispersive medium.

The applicability of the approach to other bubbly waters has been estimated for different propagation distances and bubbly waters in large ranges of radius (0.4-4 mm) and volume fractions (0.05-0.5 %). The range of applicability is defined by $bx \simeq ayx < 0.15$ for an attenuation coefficient of the bubbly water approximated by $\tilde{\alpha}(\nu) = a(\nu/\nu_{p_0})^{-y}$, with $0.2 > y > 0$, and associated to the phase velocity $\tilde{v}(\nu)$ approximated by a $\pi\delta_x/2$ phase shift. The approach predicts a signal waveform which shape changes with x and may recover the symmetry of the source wavelet every $4/\kappa_\gamma$ meters, as a first approximation, *i.e.* about 40 m for low volume fraction of large bubbles.
Similar circumstances of bubbly waters may exist in the close vicinity of active gas seeps for instance, where bubbles can occur at volumetric void fractions as low as 0.01 % with diameters up to 4 mm and sounded by the use of a very high frequency echosounder [29]. In such natural environments, the present work may motivate future works on underwater communication by contributing to acoustic quantification of gas bubbles in the ocean water column.

References

[1] Michael A Ainslie and Timothy G Leighton. "Review of scattering and extinction cross-sections, damping factors, and resonance frequencies of a spherical gas bubble". In: *The Journal of the Acoustical Society of America* 130.5 (2011), pp. 3184–3208.

[2] Habib Ammari, Brian Fitzpatrick, David Gontier, Hyundae Lee, and Hai Zhang. "Minnaert resonances for acoustic waves in bubbly media". In: *Annales de l'Institut Henri Poincaré C, Analyse non linéaire*. Vol. 35. 7. Elsevier. 2018, pp. 1975–1998.

[3] Victor C Anderson. "Sound scattering from a fluid sphere". In: *The Journal of the Acoustical Society of America* 22.4 (1950), pp. 426–431.

[4] Keita Ando, Tim Colonius, and Christopher E Brennen. "Improvement of acoustic theory of ultrasonic waves in dilute bubbly liquids". In: *The Journal of the Acoustical Society of America* 126.3 (2009), EL69–EL74.

[5] Clarence Samuel Clay and Herman Medwin. "Acoustical oceanography: principles and applications". In: (1977).

[6] Kerry W Commander and Andrea Prosperetti. "Linear pressure waves in bubbly liquids: Comparison between theory and experiments". In: *The Journal of the Acoustical Society of America* 85.2 (1989), pp. 732–746.

[7] Martin Devaud, Thierry Hocquet, Jean-Claude Bacri, and Valentin Leroy. "The Minnaert bubble: an acoustic approach". In: *European Journal of Physics* 29.6 (2008), p. 1263.

[8] Jean-Baptiste Doc, Jean-Marc Conoir, Régis Marchiano, and Daniel Fuster. "Nonlinear acoustic propagation in bubbly liquids: Multiple scattering, softening and hardening phenomena". In: *The Journal of the Acoustical Society of America* 139.4 (2016), pp. 1703–1712.

[9] Ramani Duraiswami, Sankar Prabhukumar, and Georges L Chahine. "Bubble counting using an inverse acoustic scattering method". In: *The journal of the acoustical society of America* 104.5 (1998), pp. 2699–2717.

[10] Vincent Duro, Dominique Raphaël Rajaona, Dominique Décultot, and Gérard Maze. "Experimental study of sound propagation through bubbly water: comparison with optical measurements". In: *IEEE Journal of Oceanic Engineering* 36.1 (2011), pp. 114–125.

[11] Yuzhe Fan, Haisen Li, Chao Xu, and Tian Zhou. "Influence of bubble distributions on the propagation of linear waves in polydisperse bubbly liquids". In: *The Journal of the Acoustical Society of America* 145.1 (2019), pp. 16–25.

[12] L.L. Foldy. "The multiple scattering of waves". In: *Phys. Rev.* 67 (1945), pp. 107–119.

[13] Francis E Fox, Stanley R Curley, and Glenn S Larson. "Phase velocity and absorption measurements in water containing air bubbles". In: *The journal of the acoustical society of America* 27.3 (1955), pp. 534–539.

[14] Peter JA Frinking, Nico de Jong, and E Ignacio Cespedes. "Scattering properties of encapsulated gas bubbles at high ultrasound pressures". In: *The Journal of the Acoustical Society of America* 105.3 (1999), pp. 1989–1996.

[15] Daniel Fuster, Jean-Marc Conoir, and T Colonius. "Effect of direct bubble-bubble interactions on linear-wave propagation in bubbly liquids". In: *Physical Review E* 90.6 (2014), p. 063010.

[16] Walter I Futterman. "Dispersive body waves". In: *Journal of Geophysical research* 67.13 (1962), pp. 5279–5291.

[17] DE Goertz, ME Frijlink, MM Voormolen, Nico de Jong, and AFW van der Steen. "High frequency attenuation measurements of lipid encapsulated contrast agents". In: *Ultrasonics* 44 (2006), e131–e134.

[18] Lars Hoff, Per C Sontum, and Jens M Hovem. "Oscillations of polymeric microbubbles: Effect of the encapsulating shell". In: *The Journal of the Acoustical Society of America* 107.4 (2000), pp. 2272–2280.

[19] S. Ker and Y. Le Gonidec. "Fractional integration of seismic wavelets in anelastic media to recover multiscale properties of impedance discontinuities". In: *Geophysics* 83 (2018), pp. 61–71.

[20] M. Lax. "Multiple scattering of waves". In: *Rev. Mod. Phys.* 23 (1951), pp. 287–310.

[21] Y. Le Gonidec, D. Gibert, and J.-N. Proust. "Multiscale Analysis of waves reflected by complex interfaces : basic principles and experiments". In: *J. Geophys. Res.* 107.doi:10.1029/2006JB004518 (2002).

[22] V. Leroy, A. Strybulevych, and J.H. Page. "Sound velocity and attenuation in bubbly gels measured by transmission experiments". In: *J. Acoust. Soc. Am* 123 (2008), pp. 1931–1940.

[23] Bin Liang, Xinye Zou, and Jianchun Cheng. "Effective medium method for sound propagation in a soft medium containing air bubbles". In: *The Journal of the Acoustical Society of America* 124.3 (2008), pp. 1419–1429.

[24] Alexandra M Padilla and Thomas C Weber. "Acoustic backscattering observations from non-spherical gas bubbles with ka between 0.03 and 4.4". In: *The Journal of the Acoustical Society of America* 149.4 (2021), pp. 2504–2519.

[25] Jacob Rubinstein. "Bubble interaction effects on waves in bubbly liquids". In: *The Journal of the Acoustical Society of America* 77.6 (1985), pp. 2061–2066.

[26] Edward Silberman. "Sound velocity and attenuation in bubbly mixtures measured in standing wave tubes". In: *The journal of the Acoustical Society of America* 29.8 (1957), pp. 925–933.

[27] HR Suiter. "Pulse length effects on the transmissivity of bubbly water". In: *The Journal of the Acoustical Society of America* 91.3 (1992), pp. 1383–1387.

[28] Tony Valier-Brasier, Jean-Marc Conoir, Francois Coulouvrat, and Jean-Louis Thomas. "Sound propagation in dilute suspensions of spheres: Analytical comparison between coupled phase model and multiple scattering theory". In: *The Journal of the Acoustical Society of America* 138.4 (2015), pp. 2598–2612.

[29] Binbin Wang, Scott A Socolofsky, John A Breier, and Jeffrey S Seewald. "Observations of bubbles in natural seep flares at MC 118 and GC 600 using in situ quantitative imaging". In: *Journal of Geophysical Research: Oceans* 121.4 (2016), pp. 2203–2230.

[30] Y. Wang. "Generalized seismic wavelets". In: *Geophys. J. Int.* 203 (2015), pp. 1172–1178.

[31] Preston S Wilson, Ronald A Roy, and William M Carey. "Phase speed and attenuation in bubbly liquids inferred from impedance measurements near the individual bubble resonance frequency". In: *The Journal of the Acoustical Society of America* 117.4 (2005), pp. 1895–1910.

[32] Z. Ye. "Acoustic dispersion and attenuation in many spherical scatterer systems and the kramers-Kronig relations". In: *J. Acoust. Soc. Am.* 101 (1997), pp. 3299–3305.